A Fast Prediction Algorithm of Satellite Passes

P. L. Palmer & Yan Mai

Surrey Space Centre
University of Surrey,Guildford,GU2 7XH, UK
Tel +44 1483 259278, Fax +44 1483 259503
p.palmer@eim.surrey.ac.uk

Abstract

Low cost, fast access and multi-functional small satellites are being increasingly used to provide and exchange information for a wide variety of professions. They are particularly useful, for example, as a resource in very remote areas where they can provide useful information such as to rescue teams for changing conditions in a disaster zone and monitoring the sea state to warn approaching shipping. Unlike terrestrial communication systems, the receiver/transmitter in these different application areas needs to be powered on and contact to specialised satellites to exchange data at specific time rather than consuming valuable power at all the time. This, therefore, requires accurate knowledge of when these satellites will pass over the horizon of the given location over a timescale of months in some cases. On the other hand, long term orbit estimation with high accuracy is also a key part for mission analysis and Earth observation operation planning. The same algorithm is also needed onboard satellites for autonomous on-board data management. The principal difficulty of predicting satellite passes over such long timescales is to take account of the effects of atmospheric drag.

In this paper, we present a fast algorithm for the prediction of passes of a LEO satellite over any given location which provides high accuracy over a long period. The method exploits sophisticated analytic models of the orbit and provides direct computation of rise-set times and nadir tracking without the need of orbit propagation for hill climbing. This provides for a very small fast algorithm so more suitable for low-end computers and hand-held sets. Since the atmospheric drag is the key factor that affects the accuracy for long-term estimation for satellite in LEO, this model not only includes secular perturbation and periodic perturbations, on the other hand a drag model based on the well acknowledged NASA atmosphere statistics is incorporated. Different from those in other orbit prediction methods, for example, the most widely used SGP4, the drag model here has a variable parameter which is subject to modify as time being on according to periodical atmosphere properties changing. Simulation result shows it can provide quite accurate estimation for long look-ahead period.

1 Introduction

Small satellites are becoming more and more flexible and powerful to enable military and civil applications such as low cost store-and-forward communication, remote facility metering, disaster warning for global shipping service and some Earth Observation missions. The replacement of traditional spacecraft in these applications is motivated by the reality of shrinking governmental budgets and commercial interest in deploying low-cost small satellites for a wide variety of professions.

In particular, there has been big trend to use low cost, fast access and multi-functional small satellites to provide and exchange information for a wide range of applications, which includes communication in a very remote area for changing conditions, disaster warning for approaching ships in the sea and so on. Different from ordinary communication stations which has sufficient power supply, the communication module in these applications, say, a rescue team trekking in a south American forest, has only very limited power capacity, therefore requires the receiver/transmitter to be powered on and contact to the spacecraft at specific time rather than consuming valuable power at all the time. This, therefore, requires accurate estimation of when the satellites will start to be visible (rise) to

a given location on the Earth and similarly, the time when the satellite disappears from the horizon (set), over a timescale of months in some cases. Meanwhile, long term and highly accurate orbit estimation, especially rise-and-set time computation, also plays a key part in the pre-request information for mission analysis and on-board resources management in more general communication, Earth observation and scientific spacecraft.

One conventional way to solve this problem is to let the satellite run through its ephemeris, and checking at each instant to see whether it just becomes visible/invisible to a specific ground location. An orbital propagation is advanced in time by some small time increment, Δt, and a possibility check is performed at each step, this kind of scheme is called trajectory checking. This method, however, is fairly computational expensive and therefore not suitable in the circumstances where powerful processing resources are absent. Escobal [1] proposed a faster method to solve this problem by developing a closed-form solution for the visibility periods. He introduced a single transcendental equation as a function of the *eccentric anomaly* of the satellite orbit which he called the *controlling equation*. Numerical methods were then used to find the rise and set times. The advantage of this equation is that it is solved only once per orbital period, in contrast with the hundreds of times the Keplerian equation must be solved with the standard step-by-step technique of hill climbing. The controlling equation, however, is only valid for two-body motion.

Besides the *controlling equation* method, Lawton [7] has developed another method to solve for satellite-satellite and satellite-ground station visibility periods for vehicles in circular or near circular orbits by approximating the visibility function $\psi(t)$, by a Fourier series. More recently, Alfano [8] further developed the $\psi(t)$ function to suit all orbital types. A significant difficulty, however, of predicting LEO satellite passes over long period is to take account of the effects of atmospheric drag.

In this paper, a fast algorithm for the rise-and-set time prediction for LEO satellite is proposed. It provides high accuracy over a long period. By some further extension, this algorithm also has the potential to provide maximum elevation angle time prediction (or nadir tracking problem solving), which is very useful for imaging planning using small satellites. The new method exploits sophisticated analytic models of the orbit and therefore provides direct computation of rise-set times and nadir tracking. This makes it very suitable for low-end processors in hand-held sets and computers on-board spacecraft. Furthermore, in addition to taking account of secular perturbation and periodic perturbations, this algorithm includes a straight forward atmospheric drag model derived from the well acknowledged NASA atmosphere statistics in order to overcome the difficulties involving long-term prediction without incurring complex computational overhead. Different from those in other orbit prediction methods, for example, the most widely used SGP4, the drag model here has variable parameter which is subject to modify as time being on according to periodical atmosphere properties changing. Simulation result shows this drag model works satisfactorily in prediction over long timescale.

The paper will be organised as follows: in section 2, we describe the first phase of the new method, which is called "Coarse Search", it works in two-body, secular perturbations arising from the Earth's oblateness and atmospheric drag perturbations. In section 3, we introduce the second phase of the method, which is called "Refinement" which improves the accuracy of the new method. A method to update the atmospheric drag parameter consistently for long-term prediction is addressed in section 4. Simulation results are presented in section 5, as well as the comparison of CPU processing time between the conventional method and this new method. Finally, in section 6, we set out our conclusions.

2 Coarse Search

2.1 Fundamental Algorithm - Two-Body Analysis

Figure 1: Satellite orbiting around the Earth showing crossings of the Target Latitude Line (TLL).

We can easily estimate the satellite closest approach time by checking the satellite ascending and descending passage once respectively *per day*. Set $T\ (= 2\pi/n)$

to be the *orbital period* of the satellite and t_0 the time when the satellite first crosses over a given latitude line on the ascending pass (see figure(1)). We call the circle of constant latitude that runs through the target location the *Target Latitude Line* (*TLL*). The key point of our approach is to use the fact that for two-body motion, a satellite will revisit exactly the same point in an inertial co-ordinate system after each orbital period T (see figure(1)). This means that the satellite will make another ascending-pass over the *TLL* at time $(t_0 + T)$. To simplify the discussion we shall ignore the descending passages over the *TLL* and include them again only at the end. Note, in this method, satellite position is expressed by the redundant epicycle coordinates: (r, λ, I, Ω) [2][3].

If the location of a target on the Earth is (υ_T, ϕ_T), where υ_T and ϕ_T are the geodetic longitude and latitude respectively, then the satellite will pass over the *TLL* every $t_0 + NT$ (or $t_0 + N2\pi/n$), where N is an integer representing the number of satellite passages, n is satellite's orbital mean motion.

At time t_0 the satellite is over the *TLL* and the initial *longitude* difference between the satellite footprint υ_S and target υ_T is $\Delta\upsilon = \upsilon_S - \upsilon_T$. After each orbital period the satellite revisits the *TLL* and the Earth rotates under it bringing the target closer to the satellite's longitudinal position. The satellite will see the target approaching by an amount $\omega_\oplus$T or $\omega_\oplus 2\pi/n$, where $\omega_\oplus$ is the Earth's rotation rate. The *Target-Closest-Satellite-Passage* (*TCSP*) occurs when the longitude difference $d\upsilon$ is smaller than $\omega_\oplus 2\pi/n$. Therefore we obtain the following fundamental equation:

$$\Delta\upsilon = N\omega_\oplus 2\pi/n + d\upsilon \tag{1}$$

where $d\upsilon$ is the longitudinal difference between the subsatellite point and the target at *TCSP*.

So:

$$N = \left[\frac{\Delta\upsilon}{2\pi}\frac{n}{\omega_\oplus}\right] \tag{2}$$

where square brackets implies the integer part.

In other words, the closest approach to the target will occur when $0 \leq d\upsilon < \omega_\oplus 2\pi/n$. Therefore as long as we know the initial passage time t_0 of the *TLL* and the satellite's orbital period T, we can derive the possible closest approach time over long intervals of time. We name the procedure of *TCSP* estimation as *coarse search*.

To determine the rise-and-set times of the satellite over a given ground station, we need to set an angle margin, θ_v (described in section 2.1.2). See figure(2), when satellite is visible, its longitude υ_S must satisfy the following condition:

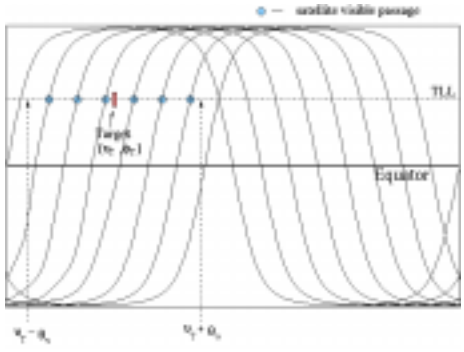

Figure 2: This figure shows the basic idea of our new method for satellite rise-and-set times. When satellite longitude is within $\upsilon_T - \theta_v$ and $\upsilon_T + \theta_v$, the passes are visible.

$$\upsilon_T - \theta_v \leq \upsilon_S \leq \upsilon_T + \theta_v \tag{3}$$

In order to test whether the passes are visible, we start from $\upsilon_S \simeq \upsilon_T - \theta_v$, if this is a visible pass we add it to our coarse search list. When $\upsilon_S < \upsilon_T - \theta_v$ we add 2π to υ_S. When $\upsilon_S > \upsilon_T + \theta_v$ we can compute the difference in longitude $\Delta\upsilon_v = \upsilon_S - (\upsilon_T + \theta_v)$ that will bring it to within the visibility of the ground station. Therefore we get the following formula for satellite visible estimation:

$$N = \left[\frac{\Delta\upsilon_v}{2\pi}\frac{n}{\omega_\oplus}\right] + 1 \tag{4}$$

2.1.1 *Finding Initialisation Argument of Latitude* λ_0

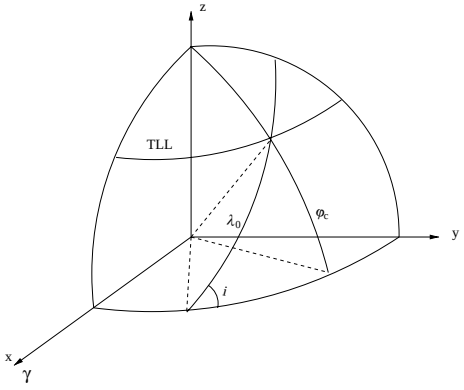

Figure 3: Geometry of λ_0 in ECI coordinate. i is the orbit inclination and φ_c is the target latitude.

In the previous section, we pointed out that we need to know the initial passage time t_0 of the *TLL*. In our approach, we only need to calculate the corresponding initial υ_{S0}. Therefore we need λ_0 (the initial argument of latitude) for *TLL*. This is found from the spherical triangle shown in figure(3).

$$\sin\lambda_0 = \frac{\sin\varphi_C}{\sin I} \tag{5}$$

2.1.2 *The Longitudinal Offset Angle Margin*

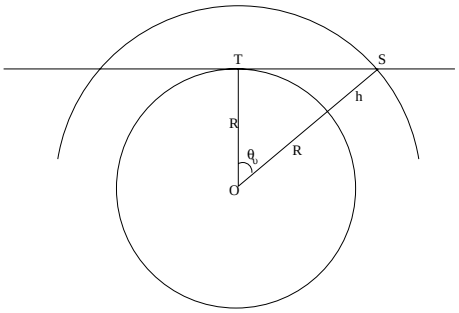

Figure 4: This figure shows within longitude angle θ_v satellite is visible to the ground target.

The rise time of a satellite should occur when the satellite, at a given orbital height, crosses the horizon plane. In this case we set up another angle margin θ_v as shown in figure(4) and simplified the calculation for it.

If the orbital radius of the satellite S is $a(= R + h)$ then:

$$\cos\theta_v = \frac{R}{a} \tag{6}$$

We therefore wish to estimate the times when the satellite reaches the target longitude within $\pm\theta_v$. However, because this a simplified calculation for satellite longitudal angle margin, to avoid missing some low passes we reduce R by a fixed fraction.

2.2 Adding Secular Perturbations

A satellite under the influence of an inverse square gravitational law has truly constant orbital elements. In reality, however, there is a gradual change in the orbital elements due to the Earth's oblateness. The principal effect of this is to introduce a short period oscillation of the orbital elements, which we can ignore in most cases. The argument of perigee, ω, and longitude of the ascending node, Ω, however, experience a secular drift which significantly changes the long term prediction of maximum elevation angle. We can adopt the method we have outlined in section 2.1 to take proper account of all these secular variations. In the following description we will introduce the formulae for satellite rise-and-set times.

Firstly we can easily add secular perturbations to the *coarse search* procedure for the effect on argument of latitude λ which changes the *nodal period* of satellite comes back to the same *TLL*:

$$\lambda = \alpha(1 + \kappa) \tag{7}$$

where κ is the coefficient of secular drifts in the epicycle equations [2] and $\alpha = nt$. So there is a change in α for each TLL crossing of $\Delta\alpha = 2\pi/(1 + \kappa)$.

The second effect is the precession of the orbital plane ($\dot{\Omega}$). This moves the target away from the orbital plane ($\dot{\Omega} > 0$). We can incorporate this effect into the rotation rate of the Earth.

$$\omega_{eff} = \omega_\oplus - \dot{\Omega} \tag{8}$$

In the epicycle description of the orbit[2], the variation in Ω is expressed as:

$$\Omega = \Omega_0 + \theta\alpha \tag{9}$$

where θ is the secular coefficient of plane precession[2][3]. Hence $\dot{\Omega} = \theta n$

We can incorporate these results into equations (1) and (2) for the *coarse search* to get:

$$\Delta\upsilon = (\omega_\oplus - \theta n) N \frac{\Delta\alpha}{n} \tag{10}$$

Therefore:

$$N = \left[\frac{\Delta\upsilon}{2\pi}\frac{n(1+\kappa)}{(\omega_\oplus - \theta n)}\right] + 1 \tag{11}$$

2.3 Accounting for Drag

Gravity is not the only force acting on the satellite. The most important other effect comes from the Earth's atmosphere, which still has a significant effect on orbits up to altitudes as high as 1000km. Because most of our small satellites orbit at altitudes lower than this, we need to consider the effects of atmospheric drag. Drag is very difficult to model because of the many factors affecting the Earth's upper atmosphere and the satellite's attitude which affects the cross sectional area. In this paper, we only consider the effect of drag on the

satellite's argument of lattitude for the *coarse search* and include the effect on r in the *refinement*. In order to test our result, the SGP4 model[10] has been used for drag modelling.

The effect of drag on the argument of latitude can be incorporated into the epicycle equations as:

$$\lambda = \alpha(1+\kappa) + 1.5B\alpha^2 \tag{12}$$

where B is the drag coefficient.

We start by finding the change in the epicycle phase α over one nodal period. By setting λ to be 2π we find the solution for $\alpha(=\Delta\alpha)$ from equation (12):

$$\Delta\alpha = \frac{4\pi}{1+\kappa} \cdot \frac{1}{1+\sqrt{1+12\pi B}} \tag{13}$$

Using this in equation (10) we obtain:

$$N = \left[\frac{\Delta\upsilon}{\Delta\alpha}\left(\frac{n}{\omega_\oplus - \theta n}\right)\right] + 1 \tag{14}$$

This completes our discussion of the *coarse search* where we have included the secular perturbations and atmospheric drag.

3 Refinement

Having estimated the approach time to the target at *TLL*, we now need a procedure that will refine this estimate to an application set tolerance. For this we extend Escobal's [1] approach to determine the rise-and-set time, by introducing a new *controlling equation* based on the epicycle equations.

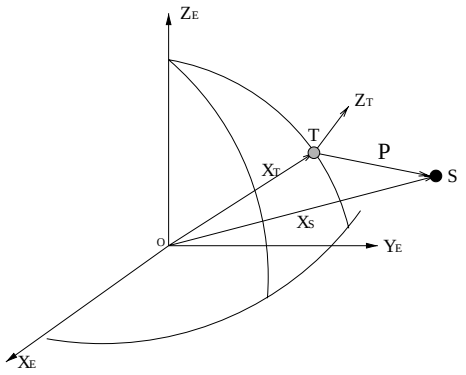

Figure 5: This figure describes the geometry of ground target (T) and satellite (S) in ECEF coordinate.

In figure(5), we show the geometry of a satellite pass. The target ground station, T, is located on the surface of an oblate Earth, and the vector $\vec{z}_T$ is the local normal to the ground target surface. The position of the satellite is S. We have the position of both the target and the satellite in Earth centred, Earth fixed (ECEF) coordinates [5] expressed in r, I, Ω, λ, α from the epicycle equations, from which we compute the slant vector $\vec{P}$:

$$\vec{P} = \vec{X}_S - \vec{X}_T \tag{15}$$

This gives the position of the satellite as seen from the target. The elevation angle is the angle measured from the horizon up to the satellite. If this angle is h, then:

$$\vec{P} \cdot \vec{Z}_T = P \sin h \tag{16}$$

Therefore, we name a new *controlling equation*:

$$F(\alpha) = \sin h = \frac{\vec{P} \cdot \vec{Z}_T}{P} \tag{17}$$

F is a function of α only through $\vec{X}_s$; while $\vec{Z}_T$ and $\vec{X}_T$ are constant vectors in the ECEF coordinate system. $\vec{X}_s$ varies with α both because the satellite moves along its orbits and through the Earth's rotation in the transformation from ECI to ECEF coordinates. It is obvious that the *zero* points of the elevation angle h represents the *zero* of function $F(\alpha)$. Therefore, to find the rise-and-set time we just need to find α_0 such that $F(\alpha) = 0$.

3.1 Computation of Satellite location $\vec{X}_S$

The epicycle equations which express (r, I, Ω, λ) as functions of time can be written as:

$$\begin{aligned} r &= a(1+\rho) - A\cos(\alpha - \alpha_p) + a\chi\sin\beta \qquad (18)\\ &+ a\Delta_r \cos 2\beta - 2B\beta \\ I &= I_0 + \Delta_I(1-\cos 2\alpha) \qquad (19)\\ \Omega &= \Omega_0 + \theta\alpha + \Delta_\lambda \sin 2\alpha \qquad (20)\\ \lambda &= \beta + \frac{2A}{2}[\sin(\alpha-\alpha_p) + \sin\alpha_p] \qquad (21)\\ &- 2\chi(1-\cos\beta) + \Delta_\lambda \sin 2\beta + \frac{3}{2}B\beta^2 \end{aligned}$$

where we have included the effects of atmospheric drag [paper in preparation], and

$$\beta = (1+\kappa)\alpha \tag{22}$$

ρ, κ and θ are the coefficients for secular perturbation; χ is long periodic perturbation coefficients; Δ represents the short periodic terms; B is the epicycle drag coefficient.

We define the satellite position (ξ, η) on the orbital plane using Cartesian co-ordinates with the ξ axis along the ascending node of the orbit. Hence:

$$\begin{aligned} \xi &= r\cos\lambda \\ \eta &= r\sin\lambda \end{aligned}$$

$\vec{X}_S$ can be expressed in ECEF coordinates as $\vec{X}_S = (X_E, Y_E, Z_E)$, where:

$$\begin{cases} X_E = \xi\cos(\nu-\Omega) + \eta\cos I\sin(\nu-\Omega) \\ Y_E = -\xi\sin(\nu-\Omega) + \eta\cos I\cos(\nu-\Omega) \\ Z_E = \eta\sin I \end{cases} \quad (23)$$

and ν is the local ephemeris time (the angle between the first point of Aries γ and the X_E axis in the ECEF frame). These equations together describe the dependence of F on α.

4 Drag Variability Modelling

The predictions for satellite passes over long timescales are sensitive to the effects of atmospheric drag. Although we have taken account of the drag modelling the variability of the drag causes significant timing errors for satellite passes over long look ahead times. In order to reduce the variability of atmospheric drag we have averaged the historic drag data over time windows to smooth it. The smoothed drag data then represents real variability in the drag effect on the satellites, and we have assumed that this historic record is a reasonably accurate model for future variability. The drag model we have employed so far uses a constant drag coefficient. This drag coefficient represents the average drag rate over the look ahead time. In reality, however, the drag rate has some probability density distribution and this is represented by the tabulated drag rates from smoothing the drag data in time windows. As long as the look ahead time is much longer than the window size over which we have averaged, the distribution of drag rate for the prediction should accurately reflect the true drag distribution. Figure (6) and (7) show the probability density distribution for both the historic drag data and the smoothed data. We can see that for the one year look ahead time, the probability distribution of smoothed drag data is very similar as the real data. This confirms that for a single pass prediction over the look ahead time, smoothed drag data we will use has a similar distribution as the real drag data.

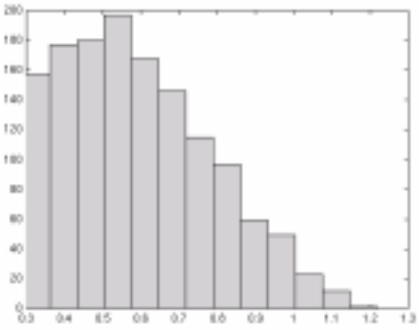

Figure 6: This figure shows the probability density distribution of real drag data for NOAA-10 satellite from 1/94 to 12/97 exclusive solar maximum.

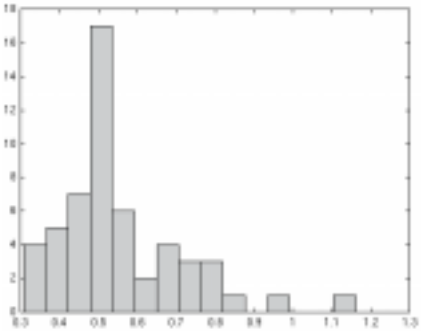

Figure 7: This figure shows the probability density distribution of one-month smoothed drag data for NOAA-10 satellite over a look ahead time of 1 year.

We now show how the epicycle model can cope with a distribution of drag rates. Let the length of the time window over which we average be dT and suppose that the historic data record starts at a time t_0 (see figure(8)). At some later epoch t_N we read the NORAD 2-line element. We can define a dimensionless time from the start epoch t_0: $\delta = n(t-t_0)$. When $t = t_N$, $\delta = \delta_N$. If we define $d\Delta = ndT$ then we can determine which element of the table $B[k]$ is appropriate for a given epoch t from: $k = \left[\frac{\delta}{d\Delta}\right]$. We also define a dimensionless time from the Norad epoch t_N as: $\alpha = n(t-t_N)$. This is the time we have used in the epicycle equations described in the previous section.

We start by considering the drag as the average drag rate over the look ahead time. Let us denote this by $\bar{B}$. We replace the symbol α by υ for this constant drag rate model. Replacing this into equation (21) and ignoring periodic terms gives:

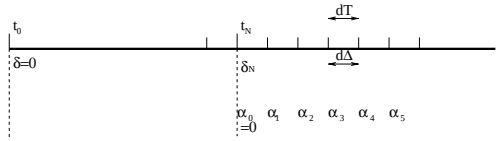

Figure 8: This figure shows the time blocks for long term prediction.

$$\lambda = (1+\kappa)\upsilon + \frac{3}{2}\bar{B}\upsilon^2 \tag{24}$$

where υ=0 when $\alpha = \alpha_0 = 0$. To relate α and υ we wish λ to be fixed -ie satellite position should be kept consistent:

$$(1+\kappa)\upsilon + \frac{3}{2}\bar{B}\upsilon^2 = \tag{25}$$
$$(1+\kappa)\alpha + 3\alpha\int_{\alpha_0}^{\alpha} B(\alpha')d\alpha' - 3\int_{\alpha_0}^{\alpha} B(\alpha')\alpha' d\alpha'$$

So if B is constant, then $\alpha = \upsilon$. To check for α we replace the integral by a sum, with intervals dT or $d\Delta$.

Let $I = 3\alpha\int_{\alpha_0}^{\alpha} B(\alpha')d\alpha' - 3\int_{\alpha_0}^{\alpha} B(\alpha')\alpha' d\alpha'$. If $\alpha_0 < \alpha < \alpha_1$, then $B(\alpha') = B[k]$, where $\alpha_0 = 0$:

$$I = \frac{3}{2}B[k]\alpha^2$$

If $\alpha_m < \alpha < \alpha_{m+1}$, then we have:

$$\begin{aligned} I &= 3\alpha[\sum_{r=0}^{m-1} B[k+r](\alpha_{r+1}-\alpha_r) \\ &+ B[k+m](\alpha-\alpha_m)] \\ &- \frac{3}{2}[\sum_{r=0}^{m-1} B[k+r](\alpha_{r+1}^2-\alpha_r^2) \\ &+ B[k+m](\alpha^2-\alpha_m^2)] \end{aligned} \tag{26}$$

The range of α can be determined as follows:

Given an input value of α we compute $\delta = \alpha + \delta_N$, then compute:

$$n = \left[\frac{\alpha+\delta_N}{d\Delta}\right];\quad n \geq k$$

If $n = k$:

$$I = \frac{3}{2}B[n]\alpha^2$$

If $n > k$:

$$\begin{aligned} I &= 3\alpha[\sum_{r=k}^{n-1} B[r](\alpha_{r-k+1}-\alpha_{r-k}) \\ &+ B[n](\alpha-\alpha_{n-k})] \\ &- \frac{3}{2}[\sum_{r=k}^{n-1} B[r](\alpha_{r-k+1}^2-\alpha_{r-k}^2) \\ &+ B[n](\alpha^2-\alpha_{n-k}^2)] \end{aligned}$$

We can write equation (26) as:

$$(1+\kappa)\upsilon + \frac{3}{2}\bar{B}\upsilon^2 = \frac{3}{2}B[n]\alpha^2 + Y_n\alpha + X_n \tag{27}$$

Let:

$$\begin{aligned} X_n &= \frac{3}{2}B[n]\alpha_{n-k}^2 \\ &- \frac{3}{2}\sum_{r=k}^{n-1} B[r](\alpha_{r-k+1}^2-\alpha_{r-k}^2) \\ Y_n &= 1+\kappa-3B[n]\alpha_{n-k} \\ &+ 3\sum_{r=k}^{n-1} B[r](\alpha_{r-k+1}-\alpha_{r-k}) \end{aligned}$$

Then we will have

$$X_{n+1} - X_n = \frac{3}{2}\alpha_{n-k+1}(B[n+1]-B[n]) \tag{28}$$
$$Y_{n+1} - Y_n = -3\alpha_{n-k+1}(B[n+1]-B[n]) \tag{29}$$

So we keep track of the current value of n and when $n > n_0$, we increment X and Y using the above relation.

$$\begin{aligned} \alpha_{n-k} &= \alpha_0 + (n-k)d\Delta \\ \alpha_{n+1} &= \alpha_n + d\Delta \end{aligned}$$

From equation (27), we can compute α from υ. Because:

$$(1+\kappa)\upsilon + \frac{3}{2}\bar{B}\upsilon^2 = \frac{3}{2}B\alpha^2 + Y\alpha + X$$

Therefore:

$$\alpha = \frac{2X - 2(1+\kappa)\upsilon - 3B\upsilon^2}{\sqrt{Y^2 + 3B(2X - 2(1+\kappa)\upsilon - 3B\upsilon^2)} + Y} \tag{30}$$

5 Test and Result

5.1 Results for Two-body and Secular Perturbation Expansion

For many practical problems, the approximation of two-body motion is sufficient, especially if two closely neighbouring points on a trajectory are under investigation.

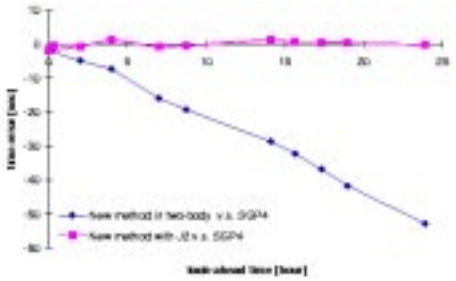

Figure 9: The black curve shows the timing error of the two-body prediction when compared with the SGP4 model, while the grey curve shows the error when J_2 is incorporated.

However, in our case for the long term prediction of satellite passes for communication, we could not ignore the cumulative effect of the gradual variation of elements from their two-body values. In figure(9) we show the prediction of our method compared with the SGP4 model [10], the black curve clearly indicates that only after a few *hours* the timing error of our prediction based on two-body theory is already up to 8 seconds, and within one day the timing error is around one minute!

To reduce the timing errors, we have included the secular effects into our *coarse search*. Unlike Escobal's original *controlling equation* our function $F(\alpha)$ not only includes secular drift but also has short-and-long periodic perturbations taken into account. We present in table(1) a comparison of the epicycle prediction with an accurate propagator [15] to look at the timing errors from the prediction when atmospheric drag is ignored. This table shows that the timing errors are as small as 0.15 seconds for a look-ahead time of almost 300 days.

Look-ahead Time [day]	Timing Error [sec]
0.96	8.7e-3
4.53	2.2e-2
9.26	3.8e-2
...	...
298.99	1.5e-1

Table 1: Table of timing errors as a function of look-ahead time, comparing the predictions with an accurate orbit propagator.

In figure(10) we show a comparison of our prediction with SGP4, using an exhaustive search approach we see that the timing difference between our method and SGP4 is less than one second for two months look-ahead time. As pointed out in [16], when atmospheric drag can be ignored the difference between our prediction and SGP4 arises from the fact that the accuracy of SGP4 is only 10^{-6} and there is a small drift of λ between the epicycle equations and SGP4 which builds up to a significant error. This demonstrates that over a look-ahead time of a few days, when drag effects can be ignored, we have achieved one-second timing accuracy.

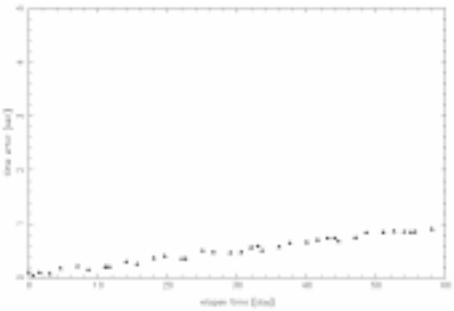

Figure 10: This figure shows timing errors when short and long variations are included, when comparing with SGP4.

5.2 Results for Including Atmospheric Drag

We next consider the drag compensation that we introduced in section 2 and 3. In figure(11), we show the timing errors compared with SGP4, now with drag included in the model. Both predictions are based on the same set of initial conditions taken for the same NORAD file and the prediction extend over 100 days. With a look-ahead time of 100 days, the timing error has now been reduced to about 2 seconds, while without drag compensation, for the same accuracy level, the look-ahead time is only one week. So for communication applications, we can predict rise-and-set times for up to one month with sufficient accuracy.

To remove the drift errors in SGP4 we performed one another experiment where we compared the predictions of our algorithm with itself, using two different NORAD files. The separation in time between the two NORAD files was anything up to 40 days, and the timing errors for the SAME pass are shown in figure(12). One of these predictions was based upon a NORAD data set from just before the pass. The dates used for this experiment were from May to July of 1997. The variability in prediction time is due to the variability of atmospheric drag.

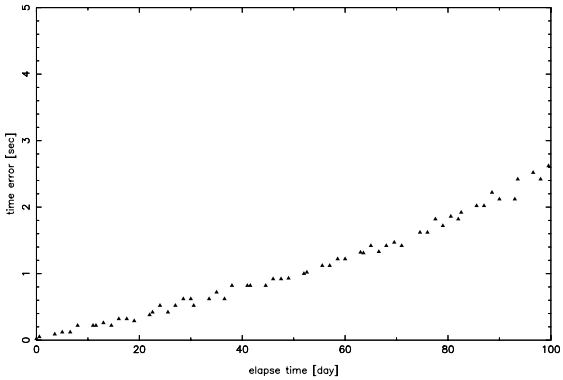

Figure 11: This figure shows timing errors when atmospheric drag is included, when comparing with SGP4.

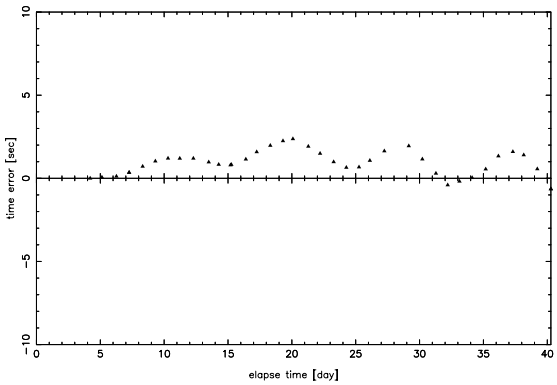

Figure 12: This figure shows the prediction errors of a single pass using our method, for look-ahead times of up to 40 days using NORAD data at different epochs.

5.3 Test and Result for Drag Variability Modelling

Although this method is targeted for small satellite application, we mainly use NOAA satellites data to test the performance for long term prediction. This is because: 1) this satellite family has very typical 800-900km Sun Synchronous Orbit, which is common for small satellites. 2) NOAA satellites have fairly complete back data log over long period which is suitable for this test. In particular, we performed the major tests on NOAA-10 as this satellite has remained in orbit for longer than 11 years and therefore the historic record of NORAD data covers a complete solar cycle. This enables us to test the performance of the method at different phases of the solar cycle.

The experiments performed consisted of fixing a particular pass on a particular day and trying to predict the time of this pass using different NORAD 2 line elements from the historical archive ranging from 1 day before hand to 550 days before hand. The results of each of these experiments are presented in the form of two graphs, figure (13), (14), (15). The first one shows a histogram of the timing errors. The second one displays the timing error for each prediction as a function of look ahead time. All the timing errors are expressed in minutes and the look ahead times are in days.

A large number of experiments were performed, but here we only present a selection of the results while other results show consistent trend as these presented ones:

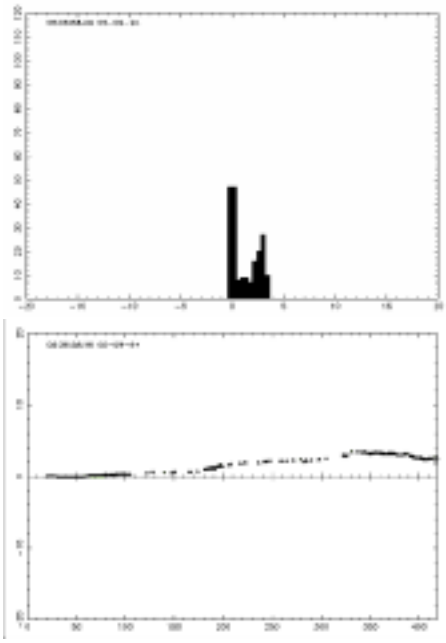

Figure 13: Histogram of timing errors and timing errors as a function of look ahead time for a pass in September 1994.

September 1994 This experiment was chosen because the 18 months prior to September 1994 all lie in the period of solar minimum. In this case the drag rate on the satellites remains fairly stable and so good estimates of the pass times are expected. The results in figures (13) show that prediction times for this pass are accurate to within 4 minutes over the 18 month interval.

March 1995 This experiment also covers the period of solar minimum, and so represents a fairly stable drag regime. During this period, however, the NORAD elements showed some drag variation which has caused

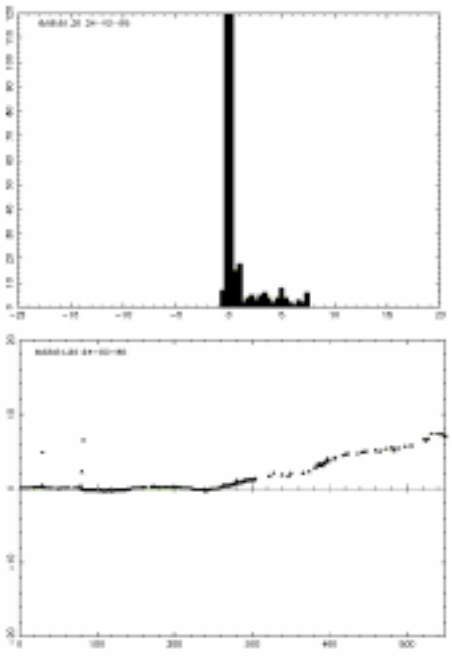

Figure 14: Histogram of timing errors and timing errors as a function of look ahead time for a pass in March 1995.

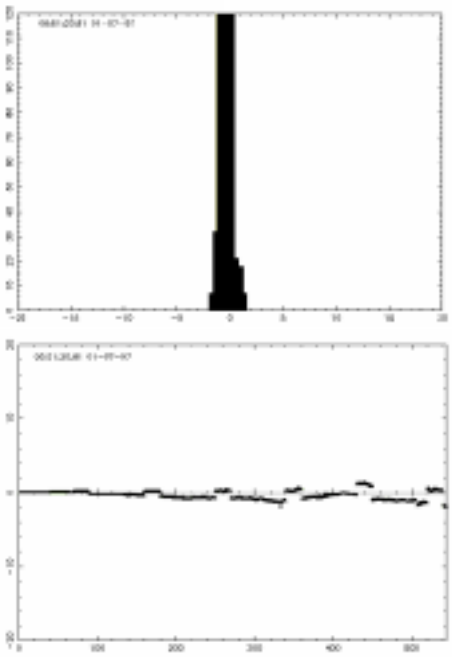

Figure 15: Histogram of timing errors and timing errors as a function of look ahead time for a pass in July 1997.

the prediction times, for long term predictions, to increase to 8 minutes in 18 months. The results are still accurate to within 2 minutes for over 1 year look ahead time. The histogram shown in figure (14) shows a very strong peak at small times.

July 1997 Another example of a prediction during solar minimum was the July 1997 pass. In figure (15) we show once again similar results to the previous experiment. These results were the best case found and show timing errors less than 1 minute over 18 months. The plot as a function of look ahead time shows a series of sudden jumps. This is an artifact of the simple median filtering that has been done on the historic drag data.

We then continued this experiment to show the prediction errors for look ahead times of up to 3 years. The results of this extended experiment are presented in figure (16) as a function of look ahead time. We see from this experiment that predictions of order 4 minutes can be maintained over this time period. These experiments provide a fair representation of performance during solar minimum.

June 1993 After couple of experiments concerning solar minimum period, the next experiment extends back into the previous solar maximum. Therefore, for long look ahead time, fairly rapid changes in the drag rate were experienced by the satellite. We can see the effect of this on the prediction data in upper graph of figure (17), in which drag parameter is a constant. The graph shows that the timing error increases rapidly after 80 days. It means from the begining we have over estimated the drag parameter because the previous period was in solar maximum. However, after we modelled drag using the method introduced in section 4, the lower graph of figure (17) clearly shows the timing accuracy has been greatly improved. By adjusting the drag parameter according to the smoothed drag statistic data, we avoided over-estimating drag parameter too much - the prediction timing error is reduced to less than 4 minutes after 300 days even when solar maximum period is included. Therefore above experiment confirms that this drag modelling method has substaintially decreased the effect of the variability of atmospheric drag.

Above experiments show that the long term prediction of satellite passes over a given ground target can be made to high accuracy even for long look ahead times up to 18 months or more. This kind of performance, indeed, is satisfactory to low-cost communication applications as addressed in the introduction.

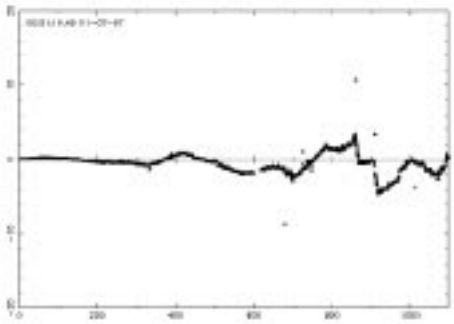

Figure 16: The timing errors as a function of look ahead time for a 3 year prediction.

5.4 Result for Computation Time

The algorithm is several order of magnitude faster to run than the exhaustive search using SGP4 we have employed. In table(2) we present some timings for the estimation on a Pentium II. These timings are sufficiently short for this algorithm to be used on hand held receivers and are sufficiently accurate to control imaging devices on satellites.

Current Programme	Proposed Method	
SGP4	two-body	Secular
786sec	2.86sec	**3.71sec**

Table 2: Processing time on a Pentium II, averaged over 10,000 experiments.

6 Conclusions

In this paper, we have introduced a new method to predict the passes of satellite to a specific target on the ground which is useful for solving the satellite visibility problem. We have firstly described a *coarse search* phase of this method including two-body motion, secular perturbation and atmospheric drag. We have then described the second phase – *refinement*, which uses a further developed *controlling equation* $F(\alpha) = 0$ based on the epicycle equations. We have shown that ignoring drag effects, we can achieve timing accuracies of 1 second for look-ahead times of 60days. When drag compensation is included, we provide sufficiently accurate timing estimates, on the order of a few seconds, for over one month ahead. For most low-cost communication applications using small satellites, the tolerable error is only required on the order of a few minutes, which lead this method valid to predict satellite passes

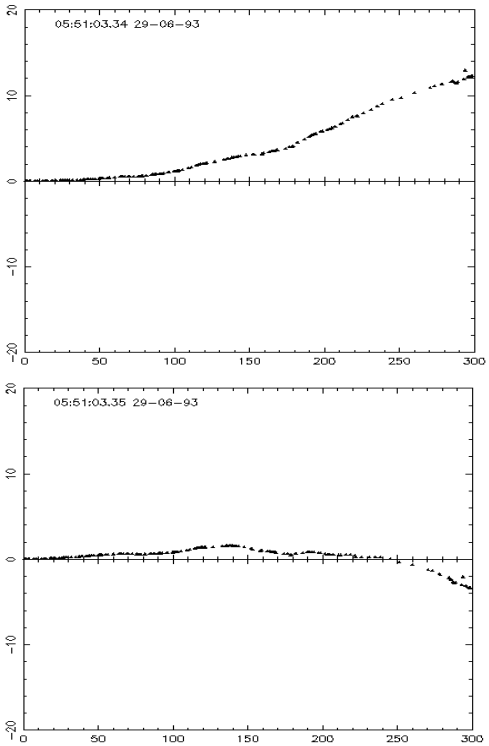

Figure 17: Timing errors for a single pass in June 1993: The upper graph shows the result when drag parameter B is a constant; The lower graph shows by using drag modelling, the timing error has been significantly reduced.

in one year period.

We have shown elsewhere [16] how to translate NORAD elements, which are freely available for all traded satellites over the Internet, to epicycle elements. Hence this method can be used by any system that has access to these NORAD files.

References

[1] Pedro Ramon Escobal, "Methods of Orbit Determination", pub. Wiley, New York, 1976.

[2] Y. Hashida & P. Palmer "Epicyclic Motion of Satellites about an Oblate Earth", submitted to AIAA J. Guidance, Control & Dynamics, 2000.

[3] Y. Hashida & P. Palmer "Post Epicyclic Motion of Satellite under J_2 Potential" submitted to AIAA J. Guidance, Control & Dynamics, 2000.

[4] Fouquet M., Sweeting M.N.,University of Surrey, UK. "Earth Observation Using Low Cost SSTL

Microsatellites", Symposium on Eearth Observation Sensors & Technology, 47^{th} IAF Congress, 7-11 October 1996, Beijing China.

[5] Vladimir A. Chobotv, "Orbital Mechanics (Second Edition)", Alexander Bell Drive, Reston, Virginia, 1996.

[6] Shea JJ, "On-orbit Determination of Focal Plane Detector Positions", Proceedings of SPIE - The International Society for Optical Engineering, Vol.2812, 1996, pp.210-220.

[7] Lawton, J.A., "Numerical Method for Rapidly Determining Satellite-Satellite and Satellite- Ground Station In-View Periods", Journal of Guidance, Navigation, and Control, Vol.10, January-February 1987, pp.32-36.

[8] Salvatore Alfano , David Negron, Jr., "Rapid Determination of Satellite Visibility Periods", The Journal of the Astronautical Sciences, Vol.40, No. 2, April-June 1992, pp.281-296.

[9] Unwin M.J., University of Surrey. "The PoSAT Microsatellite GPS Experiment", ION GPS-93.

[10] Felix R. Hoots, Ronald L. Roehrich. "Models for Propagation of NORAD Element Sets", SPACETRACK REPORT NO.3, Aerospace Defense Center, Peterson, USA.

[11] http://www.celestrak.com

[12] James R. Wertz, "Spacecraft Attitude Determination and Control", Astrophysics and Space Science Library, Volume, 1978.

[13] http://www.ulib.org/Books/Numerical_Recipes/books.html

[14] Fouquet M., Sweeting M.N., "UoSAT-12 Minisatellite for High Performance Earth Observation at Low Cost", Symposium on Earth Observation Sensors & Technology, 47th IAF Congress, 7-11 October 1996, Beijing, China.

[15] P.L. Palmer, S.J. Aarseth, S. Mikkola, and Yoshi Hashida "High Precision Integration Methods for Orbit Propagation", J. of the Astronautical Sciences, Vol. 46, No. 4, 1998.

[16] Yan Mai, P.L. Palmer, "On the Conversion of NORAD Elements to Epicycle Elements", submitted to AIAA J. Guidance, Control & Dynamics, 2000.

[17] Chen Fung-Yun, et al, "Composite Satellite System for Observation of Earth Environment and International Cooperation", IAA-96-IAA.3.3.02, 47th IAF Congress, Oct 1996, Beijng, China.

[18] M.N.Sweeting and Chen Fang-Yun, "Network of Low Cost Small Satellites for Monitoring & Mitigation of Natural Disasters", IAF-96-B.3.P215, 47th IAF Congress, Oct 1996, Beijing, China.

[19] http://www.sstl.co.uk/news/subpage_news.html